PHYSICAL REVIEW B **87**, 140301(R) (2013)

Investigation of the electromagnon excitations in the multiferroic $TbMn_2O_5$

S. Petit,[1] V. Balédent,[2] C. Doubrovsky,[2] M. B. Lepetit,[3,4] M. Greenblatt,[5] B. Wanklyn,[6] and P. Foury-Leylekian[2]

[1]*Laboratoire Léon Brillouin, CEA-CNRS UMR12, 91191 Gif-sur-Yvette Cedex, France*

[2]*Laboratoire de Physique des Solides, Université Paris-Sud, CNRS-UMR 8502, 91405 Orsay Cedex, France*

[3]*Institut Néel, 38042 Grenoble, France*

[4]*Institut Laue Langevin, 38042 Grenoble, France*

[5]*Rutgers, The State University of New Jersey, Piscataway, New Jersey 08854, USA*

[6]*Clarendon Laboratory, Oxford University, Oxford, England*

(Received 1 February 2013; published 25 April 2013)

Multiferroic materials in which magnetism and ferroelectricity coexist are a time-honored subject of study, opening the route for the next generation of electronic devices. Understanding the pronounced interplay between these properties is a current challenge, especially for the realization of multiferroic devices. One of the largest reversible magnetoelectric couplings has been evidenced in $TbMn_2O_5$, the reference compound of the so-called RMn_2O_5 multiferroics. The origin of this strong coupling has been intensively studied from the static properties. Here we report an inelastic neutron scattering investigation of the dynamic properties in this famous compound. Our work sheds light on the electromagnon, a hybrid mode theoretically predicted in multiferroics, which couples magnetic excitations with polar lattice degrees of freedom. We were able to determine in $TbMn_2O_5$ the exchange constants of a model Heisenberg Hamiltonian and to identify the spin excitation that transforms in the electromagnon on passing from the ferroelectric and magnetically collinear phase to the low temperature incommensurate and weakly ferroelectric one. Our results point to the unusual feature of the dynamic magnetoelectric coupling in this series of multiferroics.

DOI: 10.1103/PhysRevB.87.140301 PACS number(s): 75.85.+t, 63.20.−e, 71.45.Lr, 78.70.Nx

Over the past few years, "multifunctional" materials have attracted much attention, opening the route towards promising applications, especially in data storage, high-speed memories with magnetically and electrically addressable states, magnetically tunable tunnel junctions, sensors, filters, and transducers, for instance. Multiferroics, which exhibit coupled electric polarization and magnetization, are at the heart of this concept. From a theoretical point of view, this coupling originates from the combination of a complex magnetic order, due to frustration, and a strong spin-lattice coupling. Indeed, atomic displacements and ferroelectric polarization ensue from the minimization of the magnetic exchange energy and the (partial) release of the frustrated magnetic interactions.[1,2] In this context, a new kind of elementary excitation called electromagnons forms, based upon the hybridization between spin excitations (spin waves) and an electric active polar lattice vibration.

This dynamic magnetoelectric effect was investigated in the 1980's,[3] but experimentally observed only recently by optical techniques in $TbMnO_3$,[4] $DyMnO_3$,[5] $BiFeO_3$,[6] RMn_2O_5,[7] among others, and by neutron scattering in $TbMnO_3$,[4] YMn_2O_5,[8] and $YMnO_3$.[9] However, it was then found to be much more general, especially not restricted to multiferroics, with the discovery of electromagnons in *nonferroelectric* $GdMnO_3$.[10] The same holds in RMn_2O_5 compounds, where the presence of electromagnons is attested to only in the *weakly ferroelectric* magnetic incommensurate ICM_2 phase of this material, but is washed out in the ferroelectric magnetic commensurate CM phase.

To shed light on the physics leading to the formation of electromagnons, we focus on the reference compound of this series, namely, $TbMn_2O_5$. By neutron scattering experiments, we report on a detailed description of the spin excitation spectrum, and identify the "magnetic side" of the electromagnon observed in optical absorption, hence generalizing the work by Kim *et al.* on YMn_2O_5.[8] In addition, we show that the spin dynamics in the commensurate CM phase is basically identical to the one observed in the incommensurate ICM_2 phases, despite the collinear structure. The main difference comes from the precursor of the electromagnon which becomes a fully three-dimensional (3D) long-range correlated excitation below the CM-ICM_2 transition.

RMn_2O_5 compounds have been intensively studied since the recent discovery in $TbMn_2O_5$ of a huge magnetoelectric coupling allowing to reversibly flop the direction of the electric polarization by applying a magnetic field.[11] $TbMn_2O_5$ crystallizes in the centrosymetric $Pbam$ space group. It is built of $Mn^{4+}O_6$ octahedra chains running along the c axis, and connected by $Mn^{3+}O_5$ pyramids.[12] This structure creates zigzag chains of $Mn^{4+}O_6$ and $Mn^{3+}O_5$ polyhedra running along the a direction, as well as loops of five nearest-neighbor Mn spins within the (a,b) plane. On cooling, $TbMn_2O_5$ undergoes a sequence of magnetic phase transitions, a feature also observed in several other members of the RMn_2O_5 series (R = Ho, Er, Yb). Below $T_{N1} \approx 42$ K, Mn^{3+} and Mn^{4+} spins order in an incommensurate phase (ICM_1), with magnetic moments mainly oriented along the a axis and a propagation vector $Q_{ICM_1} = (1/2 - \delta, 0, 1/4 + \tau)$. With decreasing temperature, δ and τ vary in the respective ranges $0.0 \leqslant \delta \leqslant 0.01$ and $0.0 \leqslant \tau \leqslant 0.02$. Below $T_E \approx 38$ K, a commensurate state (CM) is stabilized with $Q_{CM} = (1/2, 0, 1/4)$ and magnetic moments that are still nearly collinear.[13,14] This CM phase is ferroelectric with a polarization along the b axis, essentially due to a displacement of the Mn^{3+} ions.[15–17] Below $T_{N2} \approx$ 25 K, the magnetic structure recovers its incommensurate character while a strong decrease of the electric polarization

 ©2013 American Physical Society

is observed.[18,19] In this ICM_2 phase the Mn moments are noncollinear.[19] They remain in the (a,b) plane, forming a helix along the c^* direction of the incommensurate propagating wave vector. Note that Refs. 16 and 19 report a reorientation of the Tb^{3+} magnetic moments below $T_{RE} \approx 8$ K.

High purity samples of $TbMn_2O_5$ were synthesized with the flux method described in Ref. 20. A high quality single crystal of 50 mg has been picked out and characterized by various standard techniques. Elastic neutron scattering results on this sample matched the different magnetic orders reported in the literature, as shown in Fig. 1(g). Particularly, the coexistence of both $Q_{CM} = (3/2,0,1/4)$ and $Q_{ICM_2} = (\approx 3/2,0,\approx 0.3)$ magnetic reflections in the temperature range between 15 and 25 K confirmed the first order nature of the CM-ICM_2 transition. We report here inelastic neutron scattering (INS) measurements on the very same single crystal, performed on the 2T and 4F triple axis at the Orphée-LLB neutron facility (France). The final wave vector was $k_f = 2.662$ Å^{-1} for 2T and 1.55 Å^{-1} for 4F, yielding an energy resolution of 1 and 0.25 meV, respectively. Higher order reflections were removed by graphite or beryllium filters. The polarized experiment was carried out on 4F, with a bender (before the sample) and a Heussler analyzer. The scattering plane was set to $(H,0,L)$ and we used an He closed circle cryostat to reach low temperature.

Figure 1 shows (Q,ω) contour maps of the INS intensity recorded at 17 K in the ICM_2 phase. Around 12 meV, a broad dispersionless excitation is observed, which we attribute to crystal field modes resulting from the complex oxygen environment of the Tb^{3+} ions ($4f^8$, atomic ^7F state $J = 6$, and different J_z). At lower energy transfer, we observe a dispersive band of excitations attributed to Mn spin waves. Along c^*, it forms an arch with a maximum at $\hbar\omega = 4$ meV for $L = 0$ and goes close to zero energy at the expected Bragg positions of the incommensurate ordering Q_{ICM_2} [Fig. 1(d)]. Along b^* (not shown here), the dispersion is twice as small as the dispersion along the a^* and c^* directions. With the better resolution available on 4F, we found that in the ICM_2 state, this band actually consists of two previously unresolved branches, with gaps at the zone center Q_{ICM_2} of $\omega_{0exp.} = 0.8$ meV and $\omega_{1exp.} = 2.5$ meV [see Figs. 1(c) and 1(f)]. The magnetic nature of the 0.8 meV mode is unambiguously confirmed by a full polarization analysis in the spin-flip (SF) channel, carried out by a polarized inelastic neutron scattering experiment [Fig. 1(h)].

Following the analysis developed in Ref. 8, we observe further that this zone center magnon at $(Q_{ICM_2},\omega_{0exp.})$ matches perfectly well the mode observed in infrared measurements at 10 cm^{-1} for the electric field of light parallel to the b axis.[7] These optical conductivities, together with dielectric constant measurements, converge to indicate the lattice origin of the infrared mode. Adding its magnetic nature asserted by our polarized INS experiment, this reveals that both lattice and magnetic degrees of freedom are involved in this mode. This dual nature appears to be characteristic of an electromagnon.

The polarized neutron scattering setup allows further to manipulate the neutron spin and in turn to determine, within this magnetic response, the contribution from spin components along the vertical b axis and from spin components perpendicular to the wave vector $\vec{Q}$ within the scattering plane. Our analysis demonstrates that the electromagnon involves correlations between spin components within the (a,b) plane.

As pointed out in Ref. 7, the electromagnon is only observed in the ICM_2 noncollinear phase and disappears at nearly 25 K, at the CM-ICM_2 phase transition. To understand this behavior, we carefully studied the evolution of the spin dynamics on warming up to the CM phase. Figure 2 shows maps of the spin dynamics in the CM phase along the a^* and c^* axis around $Q_{CM} = (3/2,0,1/4)$. At first glance, we observe similar features, namely, the same crystal field excitation around 12 meV and the two low energy magnons. A closer examination unveils that the minimum of the dispersion along

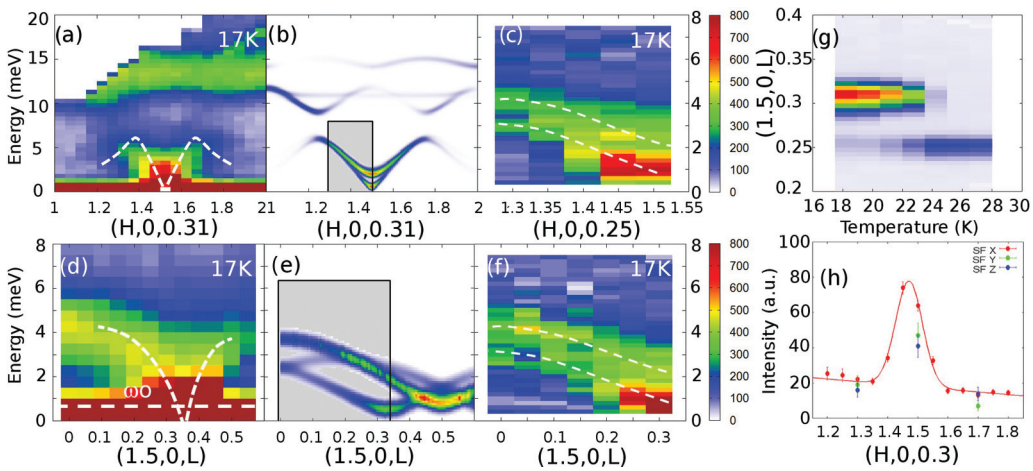

FIG. 1. (Color online) (a)–(f) Inelastic neutron scattering raw data recorded at 17 K along the $(H,0,0)$ axis [(a) and (c) performed on the 2T and 4F spectrometers, respectively] and along the $(0,0,L)$ direction [(d) on 2T and (f) on 4F] around Q_{ICM_2} and associated numerical simulations [(b) and (e)]. The shaded areas in (b) and (e) correspond to experimental maps (c) and (f), respectively. (g) Elastic neutron scattering through the CM-ICM_2 transition temperature. (h) Momentum scan along the $(H,0,0)$ direction of the 0.8 meV mode around $Q = (1.5,0,0.3)$ at 17 K and polarization analysis in the three directions of spin polarization: parallel to Q (red), parallel to $(0,K,0)$ (blue), and perpendicular to Q (green).

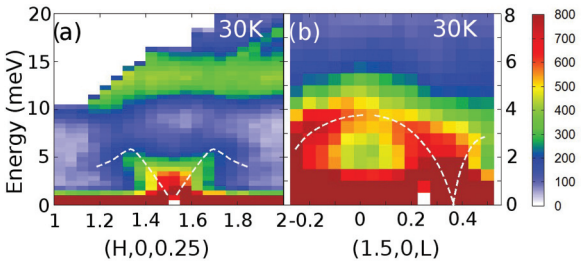

FIG. 2. (Color online) Dispersion of the magnons along the (a) $(H,0,0)$ and (b) $(0,0,L)$ directions around $Q_{CM} = (1.5,0,0.25)$ in the commensurate phase at 30 K.

c^* does not exactly locate at the CM magnetic zone center Q_{CM}, but still at Q_{ICM_2}. While in the same experiment we saw the ICM Bragg peaks vanish for the benefit of the CM Bragg reflections [see Fig. 1(g)] at 25 K, the excitation spectrum continues to originate from Q_{ICM_2} in the CM phase instead of the Q_{CM}, as expected for standard magnets. In other words, the spin dynamic remembers the ICM_2 structure even in the collinear phase. This indicates that the exchange interactions favor the incommensurate structure while the CM phase is stabilized by other forces in competition such as anisotropy or elastic effects.[21] This is further illustrated in Fig. 3 by $(H,0,L)$ maps at $\omega_{0exp.} = 0.8$ meV and energy scan at $Q = Q_{ICM_2}$ performed in both CM and ICM_2 phases. At 17 K, the electromagnon is a coherent magnon, with a well defined 3D momentum [Fig. 3(a)] and a long lifetime [Fig. 3(c)]. At 30 K, it becomes overdamped [Fig. 3(d)] and loses its correlation along c^* [Fig. 3(b)], accounting for the intensity decrease by the spread of the spectral weight in the (Q,ω) space. The inset in Fig. 3(c) shows the dispersion along c^* for the two modes at 0.8 and 2.5 meV. The dispersions stemming from $\omega_{0exp.}$ and, to a lesser extent, from $\omega_{1exp.}$ become steeper in the ICM_2 phase, providing evidence for an enhanced magnetic coupling along c^* in the ICM_2 phase. Upon heating, the electromagnon decays in an incoherent excitation, with a short lifetime and ill-defined c^* component.

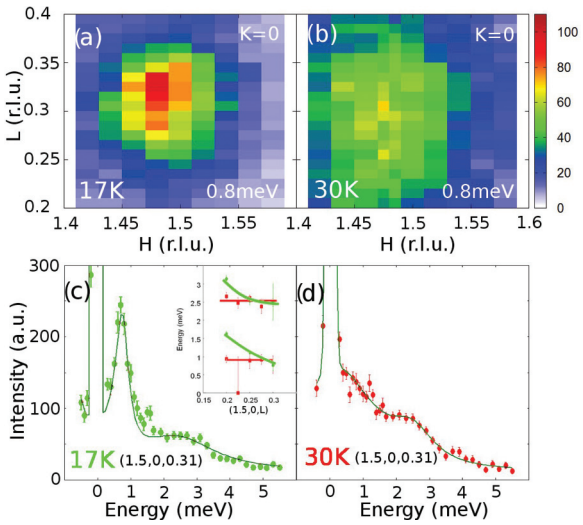

FIG. 3. (Color online) Top: Color map of inelastic scattering intensity at 0.8 meV in the $(H,0,L)$ plane in the incommensurate phase at 17 K (a) and in the commensurate phase at 30 K (b). Bottom: Energy scan on the incommensurate wave vector $Q_{ICM_2} = (1.5,0,0.31)$ in the incommensurate phase at 17 K (c) and in the commensurate phase at 30 K (d). The inset in (c) shows the dispersion at 17 K (green) and 30 K (red) along the $(0,0,L)$ direction for the two modes peaked at 0.8 and 2.5 meV.

To support this interpretation, we have numerically simulated the magnon spectrum in the ICM_2 phase using the *spin-wave* software developed at LLB, and based on the Heisenberg Hamiltonian

$$\mathcal{H} = \sum_{i,j} J_{i,j}\,\vec{S}_i \cdot \vec{S}_j + D\vec{S}_i^2, \qquad (1)$$

where the $J_{i,j}$ interactions couple spins located at ith and jth sites and D is an easy (ab) plane anisotropy term. As proposed by Chapon *et al.*,[22] five exchange constants must be considered: J_3 and J_4 couple the spins of neighboring Mn^{3+} and Mn^{4+} ions and J_5 is the coupling between two neighboring Mn^{3+} ions. J_1 and J_2 couple Mn^{4+} spins along the c direction and control the stacking of the magnetic structure along the c axis. Actually, J_2 couples spins through the Mn^{3+} layers and J_1 through the R layers (see Fig. 4). The main contribution to J_i is the antiferromagnetic Mn-Mn superexchange interaction through a shared oxygen (see Fig. 4 for the superexchange paths).

This induces a geometric magnetic frustration within loops of five Mn spins in the a,b plane. The analysis of the superexchange paths clearly shows that the dominant integrals are $\|J_5\| > \|J_4\| \gg \|J_3\|$. This leads to chains running along the a direction with an antiferromagnetic (AFM) J_4, J_5 interaction pattern weakly coupled by J_3 interactions. The J_1 and J_2

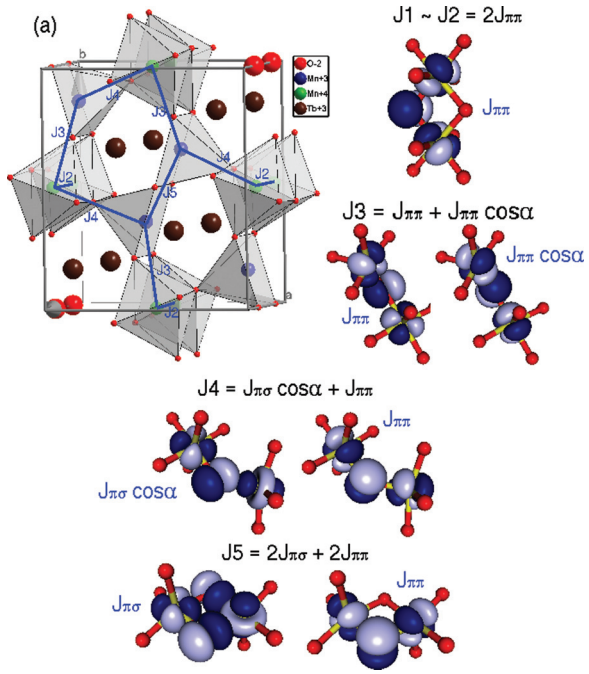

FIG. 4. (Color online) Definition of the five exchange integrals, and schematic representation of the main superexchange paths for the different magnetic integrals. The J_1 exchange constant (not shown) couples the octahedral Mn^{4+} ions between unit cells, in alternation with the J_2 exchanges that couple the same ions within the unit cell (shown).

integrals along the c direction present two superexchange paths. They can thus be expected to be antiferromagnetic, even if they are of lesser amplitude than J_5 and J_4. Despite this fact, one expects the Mn^{4+} ions related by the J_2 interaction to be ferromagnetically ordered. Indeed, the J_2 coupling is frustrated by four Mn^{4+}-Mn^{3+}-Mn^{4+} interactions associated with the large J_4 integral. The analysis for J_1 is more complex, since the contribution of the Tb^{3+} orbitals is difficult to estimate and strongly depends on the detailed distances and bond angles within the coordination polyhedra of the Tb^{3+} ions. In this picture, the dominant contribution to the magnetic energy comes from the AFM order within the chains. This order shall thus be first fulfilled. Once done, if the two chains remain symmetry related as in the *Pbam* group, the energetic contribution of J_3 sums up to zero and consequently the different orderings between the chains are degenerate. Only atomic displacements breaking the symmetry between the different chains along the b direction can lift this degeneracy, and consequently induce a polarization along the b direction. In this picture, the polarization is proportional to the scalar product of spins related by J_3 in different zigzag chains. Therefore, the relative phasing of two chains directly correlates to the magnitude of the polarization. In the CM phase, this relative phase is uniform, so that each J_3 pair contributes equally to the ferroelectricity. This is no longer valid in the ICM_2 phase owing to the incommensurability, which explains the sudden loss of ferroelectricity in this low temperature phase.

Because of the magnetic incommensurability along a and c, the low energy magnetic mode assignment requires to consider the (a,c) planes as elementary entities, weakly coupled along the b direction via J_3. For the sake of clarity we first discuss the uncoupled case corresponding to $J_3 = 0$. Since the magnetic structure involves spins rotating in the (a,b) plane, the magnetic mode involving correlations between spin components in the same (a,b) plane is the acoustic phason mode or Goldstone mode of the incommensurate magnetic structure. Another low energy mode can be identified involving spin components out of the easy magnetization plane. This mode is gapped at Q_{ICM_2} by the planar anisotropy. Next, $J_3 \neq 0$ induces optical counterparts of all these modes. This qualitative analysis has been confirmed by spin wave calculations.

Since the actual ICM_2 magnetic structure is fairly complex, we considered in the spin wave calculation, for the sake of simplicity, a commensurate magnetic unit cell $2a \times b \times 3c$, thus containing 48 coupled Mn ions. The Tb^{3+} magnetic moments have been neglected and J_3 set to zero. We found that the exchange constants $J_5 = 3.5$, $J_4 = 2.9$, $J_1 = J_2 = 0.4$ meV provide a fairly good comparison with the experimental results along the a^* and c^* directions. This is in agreement with the weakly dispersive spin waves observed along the k direction. Note that the values of J_1 and J_2 are not free parameters and depend on the assumption of a $2a \times b \times 3c$ magnetic unit cell with a magnetic structure determined in Ref. 13. These parameters are close to those found by Kim *et al.*,[8] except for J_1 and J_2, since in their model the incommensurability is due to a next-nearest-neighbor coupling J_6 and ferromagnetic J_1 and J_2.

With these parameters, a good global agreement is obtained with the data. The two low energy modes measured at $\omega_{0exp.} = 0.8$ and $\omega_{1exp.} = 2.5$ meV are calculated at $\omega_{0calc.} = 0.0$ and $\omega_{1calc.} = 2.5$ meV [Figs. 1(b) and 1(e)] and can be identified respectively as the phason mode and the out of plane rotation modes previously discussed. In our simulations, they have been found to be respectively twice and four times degenerate, a degeneracy that might be lifted by a nonzero J_3 coupling. Note that the value of $\omega_{1calc.}$ is related to the planar anisotropy gap $D = 0.13$ meV. Finally, the finite value for $\omega_{0exp.} = 0.8$ meV remains to be explained, but this gap is likely due to an easy axis anisotropy term.

Further, we speculate that fluctuations of the atomic displacements may prevent the incommensurate ordering to settle in, letting the commensurate order to establish. Their locking would in turn stabilize the helicoidal incommensurate ICM_2 phase, hence giving rise to the electromagnon as a hybrid spin and lattice mode.

In conclusion, we not only present an accurate experimental description, theoretically supported, of the electromagnon, but also shed light on its very origin. Indeed, a preexistent magnon, identified as an phason, turns into the electromagnon while acquiring c axis long-range correlations. These results provide significant information on the enigmatic electromagnon mode requiring for further theoretical investigations and opening perspectives for its confirmation in other multiferroic compounds.

[1] S. W. Cheong and M. Mostovoy, Nat. Mater. **6**, 13 (2007).
[2] H. Katsura, N. Nagaosa, and A. V. Balatsky, Phys. Rev. Lett. **95**, 057205 (2005).
[3] G. A. Smolenskii and E. Chupis, Sov. Phys. Usp. **25**, 475 (1982).
[4] A. Pimerov, A. A. Mukhin, V. Yu. Ivanov, V. D. Travkin, A. M. Balbashov, and A. Loidl, Nat. Phys. **2**, 97 (2006).
[5] N. Kida, Y. Ikebe, Y. Takahashi, J. P. He, Y. Kaneko, Y. Yamasaki, R. Shimano, T. Arima, N. Nagaosa, and Y. Tokura, Phys. Rev. B **78**, 104414 (2008).
[6] M. Cazayous, Y. Gallais, A. Sacuto, R. de Sousa, D. Lebeugle, and D. Colson, Phys. Rev. Lett. **101**, 037601 (2008).
[7] A. B. Sushkov, M. Mostovoy, R. Valdés Aguilar, S.-W. Cheong, and H. D. Drew, J. Phys.: Condens. Matter **20**, 434210 (2008).
[8] J. H. Kim, M. A. van der Vegte, A. Scaramucci, S. Artyukhin, J.-H. Chung, S. Park, S.-W. Cheong, M. Mostovoy, and S.-H. Lee, Phys. Rev. Lett. **107**, 097401 (2011).
[9] S. Petit, F. Moussa, M. Hennion, S. Pailhès, L. Pinsard-Gaudart, and A. Ivanov, Phys. Rev. Lett. **99**, 266604 (2007).
[10] A. M. Shuvaev, F. Mayr, A. Loidl, A. A. Mukhin, and A. Pimenov, Eur. Phys. J. B **80**, 351 (2011).
[11] N. Hur, S. Park, P. A. Sharma, J. S. Ahn, S. Guha and S.-W. Cheong, Nature (London) **429**, 392 (2004).

[12]J. A. Alonso, M. T. Casais, M. J. Martínez-Lope, J. L. Martínez, and M. T. Fernández-Díaz, J. Phys.: Condens. Matter **9**, 8515 (1997).
[13]G. R. Blake, L. C. Chapon, P. G. Radaelli, S. Park, N. Hur, S.-W. Cheong, and J. Rodríguez-Carvajal, Phys. Rev. B **71**, 214402 (2005)
[14]S. Kobayashi, T. Osawa, H. Kimura, Y. Noda, N. Kasahara, S. Mitsuda, and K. Kohn, J. Phys. Soc. Jpn. **73**, 3439 (2004).
[15]L. C. Chapon, G. R. Blake, M. J. Gutmann, S. Park, N. Hur, P. G. Radaelli, and S.-W. Cheong, Phys. Rev. Lett. **93**, 177402 (2004).
[16]J. Koo, C. Song, S. Ji, J.-S. Lee, J. Park, T.-H. Jang, C.-H. Yang, J.-H. Park, Y. H. Jeong, K.-B. Lee, T. Y. Koo, Y. J. Park, J.-Y. Kim, D. Wermeille, A. I. Goldman, G. Srajer, S. Park, and S.-W. Cheong, Phys. Rev. Lett. **99**, 197601 (2007).
[17]Y. Noda, H. Kimura, Y. Kamada, Y. Ishikawa, S. Kobayashi, Y. Wakabayashi, H. Sawa, N. Ikeda, and K. Kohn, J. Korean Phys. Soc. **51**, 828 (2007).
[18]G. Buisson, Phys. Status Solidi **16**, 533 (1973); **17**, 191 (1973).
[19]C. Wilkinson, P. J. Brown, and T. Chatterji, Phys. Rev. B **84**, 224422 (2011).
[20]B. Wanklyn, J. Mater. Sci. **7**, 813 (1972).
[21]R. M. Nicklow, N. Wakabayashi, M. K. Wilkinson, and R. E. Reed, Phys. Rev. Lett. **26**, 140 (1971).
[22]P. G. Radaelli and L. C. Chapon, J. Phys.: Condens. Matter. **20**, 434213 (2008).